

Inverse problem for multi-body interaction of nonlinear waves

Alessia Marruzzo¹, Payal Tyagi¹, Fabrizio Antenucci¹, Andrea Pagnani^{2,3}, Luca Leuzzi^{1,4}

¹ *Soft and Living Matter Lab.,
Rome Unit of CNR-NANONTEC,
Institute of Nanotechnology,*

Piazzale Aldo Moro 5, I-00185, Rome, Italy

² *Politecnico di Torino*

³ *HuGeF Torino*

⁴ *Dipartimento di Fisica, Università Sapienza,
Piazzale Aldo Moro 5, I-00185, Rome, Italy*

The inverse problem is studied in multi-body systems with nonlinear dynamics representing, e.g., phase-locked wave systems, standard multimode and random lasers. Using a general model for four-body interacting complex-valued variables we test two methods based on pseudolikelihood, respectively with regularization and with decimation, to determine the coupling constants from sets of measured configurations. We test statistical inference predictions for increasing number of sampled configurations and for an externally tunable *temperature*-like parameter mimicing real data noise and helping minimization procedures. Analyzed models with phasors and rotors are generalizations of problems of real-valued spherical problems (e.g., density fluctuations), discrete spins (Ising and vectorial Potts) or finite number of states (standard Potts): inference methods presented here can, then, be straightforward applied to a large class of inverse problems.

Introduction. Multi-body inference turns out to be essential whenever non-linear response is crucial for a system properties. Light mode interaction in ultra-fast multimode lasers [1–6], random lasers [7–10], multi-variable clause constrained problems [11, 12] and error correcting codes [13, 14], effective interaction among density fluctuations in heterogeneous frustrated glassy systems [15–20], fish shoals behavior [21, 22] are significant diverse examples of direct problems in which nonlinearity plays a non-perturbative role in determining the system behavior. Nevertheless, to our knowledge, not many studies of the inverse problem have been performed so far in the field. In this work we aim at filling in this gap presenting a hopefully detailed analysis based on pseudolikelihood techniques for the statistical inference in models with multi-body interactions.

Test Model. Our test model consists of N phasors a_k with a global constraint $\sum_{k=1}^N |a_k|^2 = \text{const} \times N$ (termed *spherical*) with Hamiltonian [23]

$$\mathcal{H} = -\frac{1}{8} \sum_{jklm}^{\text{d.i.}} J_{jklm} a_j a_k^* a_l a_m^* + \text{c.c.} \quad (1)$$

The a_k 's represent, e. g., the complex amplitudes of the normal modes expansion of the electromagnetic field [1]

$$\tilde{E}(\mathbf{r}, t) = \sum_k a_k(t) \mathbf{E}_k(\mathbf{r}) e^{i\omega_k t} + \text{c.c.} \quad (2)$$

characterizing the light modes in the $\mathbf{E}_k(\mathbf{r})$ basis. The amplitude $a_k(t)$ is the slowly varying coefficient of the normal mode \mathbf{E}_k of frequency ω_k and varies on time scales much slower than ω_k^{-1} . We adopt it as test model

because it is the lowest order of nonlinearity satisfying time reversal symmetry of light, as occurring, e. g., in centrometric crystals with symmetric atomic potentials [24]. The laser transition can be represented as a phase transition in statistical mechanical theory. This turns out to be possible both in ordered multimode mode-locked lasers [3, 5, 6, 25–28] and in random lasers [10, 23, 29, 30]. Considering further orders of the interaction does not change the critical behavior and the onset of the lasing regime, nor the qualitative features of the laser in the high pumping regime. We stress that, simply in order to focus the presentation, also lower order interactions (pairwise and three body) are not considered here: the sum with superscript “d.i.” in Eq. (1) is intended solely over quadruplets with distinct indices.

According to multimode laser theory [1–3, 24, 31] modes do interact nonlinearly if and only if their frequencies satisfy a frequency matching condition [5], i.e., given any four modes j, k, l, m of typical line-width γ , their angular frequencies are such that

$$|\omega_j - \omega_k + \omega_l - \omega_m| \lesssim \gamma \quad (3)$$

at least in one permutation of their indices.

With equipartite magnitudes ($|a_k| \simeq 1, \forall k$) or with quenched ones ($|a_k(t)| = A_k(0)$) Eq. (1) for phasors reduces to the so-called *XY* model for rotators, $a_j = A_j e^{i\phi_j} \rightarrow e^{i\phi_j}$, with Hamiltonian

$$\mathcal{H} = -\frac{1}{8} \sum_{jklm}^{\text{d.i.}} [J_{jklm}^R \cos(\phi_j - \phi_k + \phi_l - \phi_m) + J_{jklm}^I \sin(\phi_j - \phi_k + \phi_l - \phi_m)] \quad (4)$$

where $J^{R,I}$ are, respectively, real and imaginary parts.

We stress that the techniques here reported might be applied to any wave system with non-linear collective behavior, such as phase-locking, breathers and synchronization [32–35], including the prototype Fermi-Pasta-Ulam model [36]. Further on, the methodology can be translated, in simplified ways, to discrete variables models, like the p -clock model [28, 37] in which the rotators in Eq. (4) take only p discrete values. Properly modifying the mode interaction these p -clock models can, eventually, represent multi-body Potts models [38].

Inverse problem and inference. The inverse problem of Eq. (1) consists in determining the couplings once the variable configurations are measured. As an instance, in the optical waves framework this means quantitatively inferring the nonlinear interaction strengths given the wave emissions. Designated the theoretical model and assuming an effective equilibrium (true equilibrium or particular stationarity conditions) to infer the coupling parameters, one has to maximize the likelihood functional with respect to \mathbf{J} . For a configuration \mathbf{a} , given a set \mathbf{J} , this functional is readily introduced as

$$P(\mathbf{a}|\mathbf{J}) = \frac{1}{Z[\mathbf{J}]} \exp\{-\beta\mathcal{H}[\mathbf{a}|\mathbf{J}]\} \quad (5)$$

Computing $Z[\mathbf{J}]$ is computationally unfeasible. To circumvent this bottleneck one first defines the single variable pseudo-likelihood [39] of the values of a_i biased by all other $a_{\setminus i}$ values, besides by \mathbf{J} (see details in Sup. Mat.)

$$P_i(a_i|\mathbf{a}_{\setminus i}) = \frac{1}{Z_i[\mathbf{a}_{\setminus i}]} \exp\{a_i H_i[\mathbf{a}_{\setminus i}] + \text{c.c.}\} \quad (6)$$

with

$$H_j[\mathbf{a}_{\setminus j}] = \sum_{klm \neq j}^{\text{d.i.}} J_{jklm} \mathcal{F}_{klm} \quad (7)$$

$$\mathcal{F}_{klm} = \frac{1}{3} [a_k^* a_l a_m^* + a_k a_l^* a_m^* + a_k^* a_l^* a_m] \quad (8)$$

$$Z_i[\mathbf{a}_{\setminus i}] \equiv \sum_{a_i} \exp\{a_i H_i[\mathbf{a}_{\setminus i}] + \text{c.c.}\} \quad (9)$$

Further on, one approximates by functional computed on a finite number of independent configurations $\{\mathbf{a}^{(\mu)}\}$, $\mu = 1, \dots, M$: the log-pseudolikelihood, thus, reads

$$\mathcal{L}_i^{(0)} = \sum_{\mu=1}^M \left(a_i^\mu H_i[\mathbf{a}_{\setminus i}^\mu] + \text{c.c.} \right) - \sum_{\mu=1}^M \ln Z_i[\mathbf{a}_{\setminus i}^\mu] \quad (10)$$

Based on pseudolikelihood (PL), we adopted two methods to determine the interactions \mathbf{J} : the well known ℓ_1 -regularization [40, 41] and the most recent decimation

technique[42]. Details are reported in the Sup. Mat.

Data generation. In order to test the PL methods (PLMs) we generate data from Monte Carlo numerical simulations of the models Eq. (1) and Eq. (4). Simulated models are implemented both on sparse graphs, in which the number of interacting quadruplets scales like the number of variables, $N_q \propto N$, and on diluted dense graphs, $N_q \propto N^3$ [43]. Furthermore, we considered both strict frequency matching conditions, cf. Eq. (3), based on comb-like single mode resonance distributions ($\gamma \ll \delta\omega$), as well as *narrow-band* conditions ($\gamma > \delta\omega$). We analyze data from systems whose coupling values are randomly generated with a bimodal distribution $P(J) = 1/2[\delta(J - \hat{J}) + \delta(J + \hat{J})]$, where $\hat{J} = 1/N^{(z-1)/2}$ if the total number of quadruplets scales as $N_q \sim N^z$. This is the case, e. g., of the frustrated glassy random lasers [10, 44–48], but the methods exposed also work for the simpler cases of uniform couplings, like in standard mode-locking lasers [2, 3, 5, 28] and random couplings with a relative small fraction of negative values, e.g., random unfrustrated lasers [28, 30, 49]. We inferred data within the equilibrium hypothesis, expressed by the Boltzmann-Gibbs distribution in the likelihood functions, cf. Eq. (5), using thermalized data. The Parallel Tempering algorithm has been used to reduce thermalization times in the generated data.

Data analysis. We compare inference predictions obtained by different implementations of ℓ_1 -regularization PLM, adding to Eq. (10) a regularizing term $\mathcal{L}_i^{(0)} - \lambda \|J\|_1$, and by the decimation PLM (cf., Sup. Mat.). We consider the effects of varying the size M of data sets, as well as, the *temperature*-like parameter T .

In our analysis we minimize $-\mathcal{L}_i$, cf. Eq. (10). The codes for the PL minimization have been *ad hoc* developed with parallel programming on GPU's, reducing the running times of numerical processing with respect to C++ codes on CPU of a factor 3 for $N = 8$ up to a factor 5 for $N = 32$. In terms of timing, the parallel codes outperform the MATLAB routines [50] from a factor 15 for $N = 8$ to 30 times for $N = 16$.

Our data analysis consists in evaluating True Positive Rates (TPR) and True Negative Rates (TNR), that is the fraction of true (resp. missing) bonds also appearing (resp. absent) in the inferred set of bonds. Further on, we study the reconstruction error

$$\text{err}_J \equiv \sqrt{\frac{\sum_q (J_q - J_q^*)^2}{\sum_q J_q^2}} \quad (11)$$

yielding how far the inferred values J_q^* of the distinct quadruplets $q \equiv \{i, j, k, l\}$ are from the true values J_q . Eventually, in the decimation PLM, we analyze the behavior of the tilted pseudolikelihood function (tPLF).

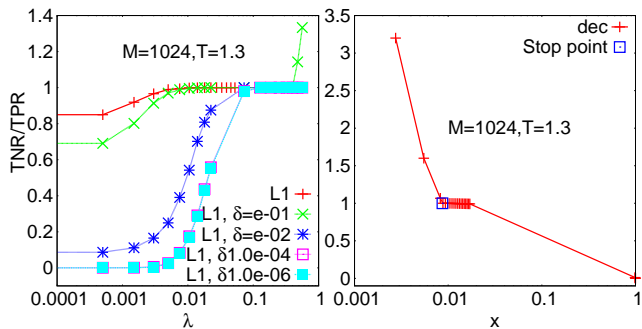


FIG. 1. The TNR/TPR ratio vs. the regularizer λ for the ℓ_1 -regularization PLM (left) and vs. the fraction x of undecimated couplings for the decimation PLM. In the latter case two different criteria are chosen to eliminate small bonds: with an *a-priori* threshold δ or by means of *a posteriori* Fisher information (see Sup. Mat.). Data are taken for the 4XY model on sparse, Erdos-Renyi-like graph with $N_q = N$, $N = 16$, $T = 1.3$, $M = 1024$.

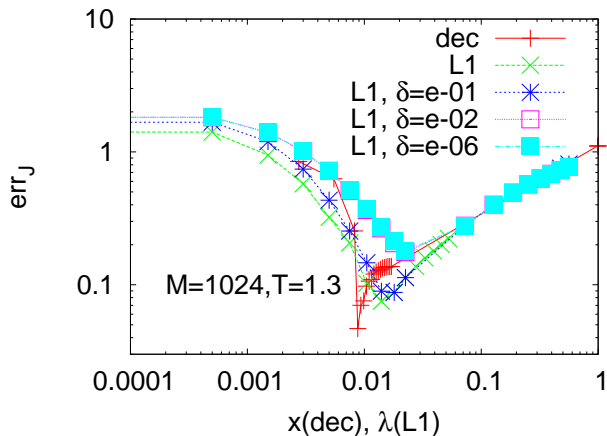


FIG. 2. Reconstruction error for the 4XY model on sparse, Erdos-Renyi-like, graph with $N_q = N = 16$, $M = 1024$ versus temperature T . The error obtained following various ℓ_1 -regularized PLMs and the decimation PLM are shown.

In Fig. 1, using data from a 4XY model on Erdos-Renyi (ER)-like sparse graph, we show how the TNR/TPR ratio increases to 1 as the parameter λ in ℓ_1 -regularization is increased when a δ -threshold criterion [41] is adopted for *model selection*, i.e., to set to zero weak couplings and reduce the number of parameters to the relevant ones. Within this criterion, the δ below which a coupling is set to zero are decided *a priori*. As λ is small, we see that the smaller the δ the less precise the network reconstruction. On the other hand, the smaller the λ the less perturbed the original PL.

If the probability distributions of the estimators are known, the issues related to an *a priori* fixing of a δ

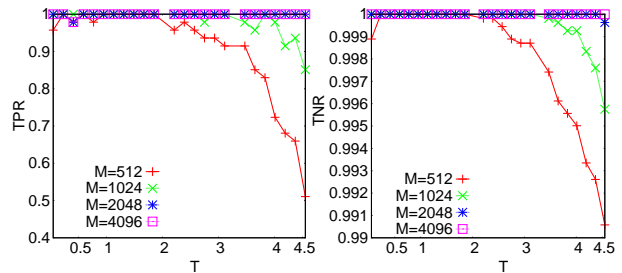


FIG. 3. TPR (Left) and TNR (Right) for decimated networks at x^M of the tPLF vs T for varying M on the 4XY model on sparse, ML-like, graphs with $N_q = 47$ ($T_c^{N \rightarrow \text{inf}} = 0$), $N = 16$.

threshold might be overcome through a more accurate *hypothesis testing* procedure. It can be seen that, as $M \rightarrow \infty$, the probability distribution of the maximum PL estimator is a Gaussian with variance given by the inverse of the Fisher information matrix [51]. Therefore, as detailed in Sup. Mat., we can construct a confidence interval for each estimated value and analyze whether it is compatible with being a zero coupling.

Always in Fig. 1 (right) we display the decimation PLM as the fraction of non-decimated couplings x increases (from fully connected limit $x = 1$ to non-interacting graph $x = 0$). At $x = 1$ the TPR is always one, for any M and T , whereas the TNR=0. As the fraction of non-decimated couplings decreases but remains greater than or equal to the true one ($x^* = 2/15$) the TPR does not decrease and the TNR increases towards one. Eventually, more couplings than those of the original network are decimated: the TPR starts decreasing and the ratio TNR/TPR consequently grows above 1 as $x \rightarrow 0$.

When comparing the performances of the most efficient regularization method with the decimation ones, we observe that the network reconstruction in terms of true and false couplings is very adequate with both methods. However, the order of magnitude of the reconstruction error, testing also the inference of the *values* of the couplings, is smaller in the decimation PLM, cf. Fig. 2, at the fraction of decimated couplings $(1 - x)$ equal to one of the true network. Within this PLM one does not have to wander along the regularizer line to find the minimum error: exact fraction of relevant parameters and best estimate of their values are contemporarily inferred. We, thus, deepen the analysis of the decimation PLM.

In Fig. 3 we display TPR (left) and TNR (right) vs. T and M for the decimated network at the maximum of the tPLF for the 4XY model on a Mode-Locked-like sparse graph. For large enough M the reconstruction is optimal for all temperatures, whereas for small M it is guaranteed only in a T interval around the finite size

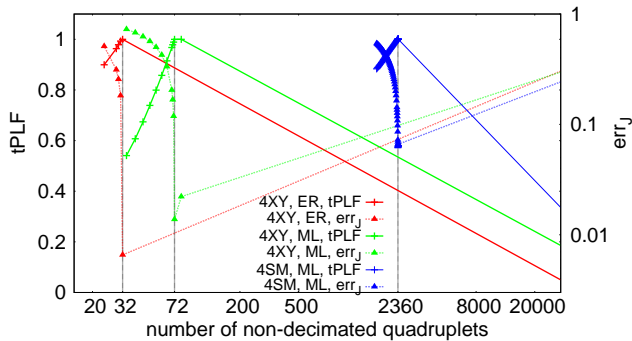


FIG. 4. Tilted PLF (normalized to its maximum) and reconstruction error for different models. Red: 4XY model on sparse, Erdos-Renyi-like graph with $N = 32, N_q = 32, M = 65000, T = 1.2$. Green: 4XY model on sparse, Mode-locked-like graph with $N = 32, N_q = 72, M = 65000, T = 1.8$. Blue: 4phasor model on dense ML graph with $N = 32, N_q = 2360, M = 65000, T = 6.2$.

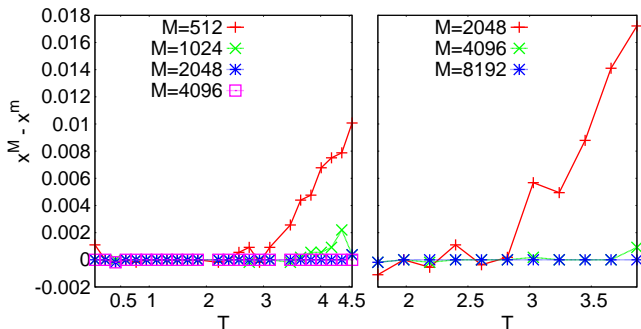


FIG. 5. Plot of the difference between the maximum of tPLF, x^M , and the minimum of the reconstruction error x^m vs T at different M for systems of $N = 16$ variables. Left: 4XY model on sparse, Mode-locked-like graph with $N_q = 47$. Right: 4phasor model on dense ML-like graph with $N_q = 252$.

critical temperature (see Sup. Mat.). The behavior of the tPLF is exemplified in three different cases in Fig. 4, where its behaviour versus x is compared to $\text{err}_j(x)$ on the same data. It is clear that, given a large enough M and/or a critical-like T the $x = x^M$ of maximum tPLF coincides with the minimum of err_j , x^m . While in determining Eq. (11), though, one needs to know the original network, in computing the tPLF measured data are sufficient. As M is small and T far from the critical region, maximum of tPLF and minimum of err_j can be mismatched, as shown in Fig. 5.

In the decimation process, x^m turns out to yield the connectivity of the original network. Tuning the external temperature-like parameter for each system studied one can identify a “critical” T interval where the reconstruction error is minimal, even orders of magnitude smaller than outside such interval. In Fig. 6 the T dependence

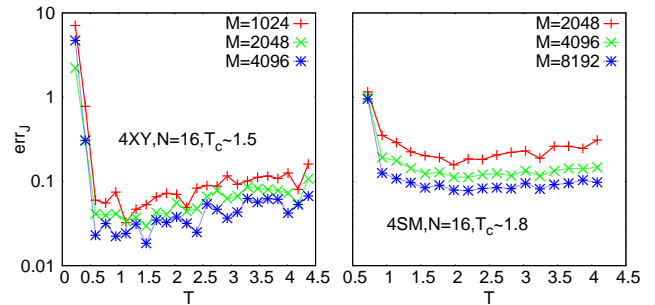


FIG. 6. Reconstruction error at its minimum $x^{\min} = x^{\text{true}}$ in the decimation procedure vs. T for various M for $N = 16$ variables systems with bimodal random values of the coupling constants. Left: 4XY model on sparse, Erdos-Renyi-like graph with $N = 16, N_q = 16$. Right: 4-phasor model on dense ML graph with $N = 16, N_q = 252$.

of err_j is plotted for the 4XY model on ER sparse graph and the 4-phasor model on ML dense graph at different values of M . As detailed in the Sup. Mat. the critical T interval turns out to be identified by the (finite size) critical temperature estimate of the phase transition point of the direct statistical mechanical problem.

Conclusions and outlook. We have been applying and improving pseudolikelihood methods to the inverse problem in multi-body models, representing systems with nonlinear response in generic theories. Our analysis has been motivated by the study of lasers in the framework of statistical mechanics, though its range of applicability is more widespread and potentially involves all problems in which nonlinear and multi-body contributions turn out to be relevant in determining the system behavior, see, e.g., [2, 9, 12–14, 17, 21]. Focusing on optics, data from experiments would allow to identify active and passive mode-locking in multimode lasers in terms of mode-coupling coefficients. When more modes on the network graph are connected by a non-vanishing coupling they are matched in frequency, cf. Eq. (3) and therefore, beyond some critical point, they will be locked in phase. Configurations of magnitudes and phases can be obtained from the Fourier analysis of the pulses in ultrafast multimode lasers [52–54], pulses known to occur because of mode-locking, and parameters like the self amplitude modulation coefficients of saturable absorbers and the Kerr parameter can be inferred. In presence of relevant light scattering, instead, occurring in random lasers, no direct measure of phases has been carried out so far, to our knowledge but only spectral intensities, i.e., modes magnitudes, are available. Once phases could be obtained, our technique would allow to discriminate whether or not mode-locking occurs in multimode random lasers, as well.

Acknowledgements. We thank Federico Ricci Tersen-

ghi for fruitful discussions. This project has received funding from the European Research Council (ERC) under the European Union's Horizon 2020 research and innovation program (Grant Agreement No. 694925).

-
- [1] M. Sargent III, M. O'Scullly, and W. E. Lamb, *Laser Physics* (Addison Wesley Publishing Company, 1978).
- [2] H. A. Haus, IEEE J. Quantum Electron. **6**, 1173 (2000).
- [3] A. Gordon and B. Fischer, Phys. Rev. Lett. **89**, 103901 (2002).
- [4] M. Katz, A. Gordon, O. Gat, and B. Fischer, Phys. Rev. Lett. **97**, 113902 (2006).
- [5] F. Antenucci, M. Ibáñez Berganza, and L. Leuzzi, Phys. Rev. A **91**, 043811 (2015).
- [6] F. Antenucci, M. Ibáñez Berganza, and L. Leuzzi, Phys. Rev. B **92**, 014204 (2015).
- [7] N. M. Lawandy, R. M. Balachandran, A. S. L. Gomes, and E. Sauvain, Nature **368**, 436 (1994).
- [8] H. Cao, Y. G. Zhao, H. C. Ong, S. T. Ho, J. Y. Dai, J. Y. Wu, and R. P. H. Chang, Appl. Phys. Lett. **73**, 3656 (1998).
- [9] D. S. Wiersma, Nature Physics **4**, 359 (2008).
- [10] F. Antenucci, C. Conti, A. Crisanti, and L. Leuzzi, Phys. Rev. Lett. **114**, 043901 (2015).
- [11] R. Monasson and R. Zecchina, Phys. Rev. E **56**, 1357 (1997).
- [12] M. Mézard, G. Parisi, and R. Zecchina, Science **297**, 812 (2002).
- [13] D. J. C. M. Kay, *Information Theory, Inference, and Learning Algorithms* (Cambridge University Press (Cambridge, UK), 2003).
- [14] M. Mézard and A. Montanari, *Information, Physics, and Computation* (Oxford University Press, 2009).
- [15] T. R. Kirkpatrick, D. Thirumalai, and P. G. Wolynes, Phys. Rev. A **40**, 1045 (1989).
- [16] A. Crisanti and H. Sommers, Z. Phys. B **87**, 341 (1992).
- [17] W. Götze, *Complex Dynamics of Glass-Forming Liquids: A Mode-Coupling Theory* (Oxford University Press (Oxford, UK), 2009).
- [18] S. Franz, G. Parisi, F. Ricci-Tersenghi, and T. Rizzo, The European Physical Journal E **34**, 1 (2011).
- [19] F. Caltagirone, U. Ferrari, L. Leuzzi, G. Parisi, F. Ricci-Tersenghi, and T. Rizzo, Phys. Rev. Lett. **108**, 085702 (2012).
- [20] U. Ferrari, L. Leuzzi, G. Parisi, and T. Rizzo, Phys. Rev. B **86**, 014204 (2012).
- [21] Y. Katz, K. Tunstrom, C. C. Ioannou, C. Huepe, and I. D. Couzin, Proc. Nat. Acad. Sci. USA **108**, 18720 (2011).
- [22] J. E. Herbert-Read, A. Pernab, R. P. Mann, D. J. T. Schaefer, T. M. Sumpter, and A. J. W. Ward, Proc. Nat. Acad. Sci. USA **108**, 18726 (2011).
- [23] F. Antenucci, A. Crisanti, and L. Leuzzi, Phys. Rev. A **91**, 053816 (2015).
- [24] R. W. Boyd, *Nonlinear Optics*, 2nd ed. (Academic Press, New York, 2002).
- [25] A. Gordon and B. Fischer, Opt. Comm. **223**, 151 (2003).
- [26] R. Weill, A. Rosen, A. Gordon, O. Gat, and B. Fischer, Phys. Rev. Lett. **95**, 013903 (2005).
- [27] R. Weill, B. Fischer, and O. Gat, Phys. Rev. Lett. **104**, 173901 (2010).
- [28] A. Marruzzo and L. Leuzzi, Phys. Rev. B **91**, 054201 (2015).
- [29] L. Angelani, C. Conti, G. Ruocco, and F. Zamponi, Phys. Rev. B **74**, 104207 (2006).
- [30] L. Leuzzi, C. Conti, V. Folli, L. Angelani, and G. Ruocco, Phys. Rev. Lett. **102**, 083901 (2009).
- [31] O. Svelto, *Principles of lasers* (Springer, 1998).
- [32] Y. Kuramoto, Lect. N. Phys. **39**, 420 (1975).
- [33] M. Antoni and S. Ruffo, Phys. Rev. E **52**, 2361 (1995).
- [34] J. A. Acebrón, L. L. Bonilla, C. J. Pérez Vicente, F. Ritort, and R. Spigler, Rev. Mod. Phys. **77**, 137 (2005).
- [35] S. Gupta, A. Campa, and S. Ruffo, J. Stat. Mech. , R08001 (2014).
- [36] E. Fermi, J. Pasta, and S. M. Ulam, LANL Report. **1940** (1955).
- [37] G. Ortiz, E. Cobenera, and Z. Nussinov, in *40 Years of Berezinskii-Kosterlitz-Thouless Theory*, edited by J. V. José (World Scientific Publisher, Singapore, 2013) Chap. 3, pp. 93–134.
- [38] R. Potts, Proc. Camb. Phil. Soc. **48**, 106 (1952).
- [39] D. Barber, *Bayesian Reasoning and Machine Learning* (Cambridge University Press (Cambridge, UK), 2012).
- [40] P. Ravikumar, M. J. Wainwright, and J. D. Lafferty, Ann. Statist. **38**, 1287 (2010).
- [41] E. Aurell and M. Ekeberg, Phys. Rev. Lett. **108**, 090201 (2012).
- [42] A. Decelle and F. Ricci-Tersenghi, Phys. Rev. Lett. **112**, 070603 (2014).
- [43] A complete dense graph would contain $O(N^4)$ interacting quadruplets.
- [44] F. Antenucci, A. Crisanti, and L. Leuzzi, Scientific Reports **5**, 16792 (2015).
- [45] A. Marruzzo and L. Leuzzi, Phys. Rev. B **93**, 094206 (2016).
- [46] N. Ghofraniha, I. Viola, F. Di Maria, G. Barbarella, G. Gigli, L. Leuzzi, and C. Conti, Nat. Commun. **6**, 6058 (2014).
- [47] A. S. L. Gomes, E. P. Raposo, A. L. Moura, S. I. Fewo, P. I. R. Pincheira, V. Jerez, L. J. Q. Maia, and C. B. de Araujo, arXiv:1509.00276 (2015).
- [48] P. I. R. Pincheira, A. F. Silva, S. J. M. Carreno, S. I. Fewo, A. L. Moura, E. P. Raposo, A. S. L. Gomes, and C. B. de Araujo, arXiv:1511.03087 (2015).
- [49] R. G. S. El-Dardiry, A. P. Mosk, O. L. Muskens, and A. Lagendijk, Phys. Rev. A **81**, 043830 (2010).
- [50] Phys. Rev. B **94**, 024203 (2016).
- [51] L. Wasserman, *All of Statistics: A concise course in statistical inference* (Springer, New York, 2003).
- [52] D. J. Kane and R. Trebino, Opt. Lett. **18**, 823 (1993).
- [53] R. Trebino, K. W. DeLong, D. N. Fittinghoff, J. N. Sweetser, M. A. Krumbügel, and D. J. Kane, Rev. Sci. Instr. **68**, 3277 (1997).
- [54] R. Trebino, *Frequency-Resolved Optical Gating: The Measurement of Ultrashort Laser Pulses*. (Springer, 2002).
- [55] A. Marruzzo, *Statistical Mechanics of continuous spin models and applications to nonlinear optics in disordered*

media (2016).

SUPPLEMENTAL MATERIAL

Pseudolikelihood function From Eq. (1) the likelihood function of a mode amplitude configuration \mathbf{a} , given a coupling set \mathbf{J} is readily introduced as

$$P(\mathbf{a}|\mathbf{J}) = \frac{1}{Z[\mathbf{J}]} \exp \{-\beta\mathcal{H}[\mathbf{a}|\mathbf{J}]\} \quad (12)$$

To construct the likelihood function of a_j , i. e., the probability distribution of a single variable given the values of all the other variables ($\mathbf{a}_{\setminus j}$), we first rewrite Eq. (1) in an equivalent way:

$$\mathcal{H}[\mathbf{a}] = -\frac{1}{8} \sum_{j=1}^N a_j H_j[\mathbf{a}_{\setminus j}] + \text{c.c.} \quad (13)$$

defining the complex-valued local effective fields

$$H_j[\mathbf{a}_{\setminus j}] = \frac{1}{4} \sum_{\substack{\text{d.i.} \\ klm \neq j}} J_{jklm} \mathcal{F}_{klm}$$

$$\mathcal{F}_{klm} = \frac{1}{3} [a_k^* a_l a_m^* + a_k a_l^* a_m^* + a_k^* a_l^* a_m]$$

Then, we separate the contributions from a given variable a_i from all contributions not involving a_i :

$$\begin{aligned} \mathcal{H}[\mathbf{a}] &= -\frac{1}{8} a_i H_i[\mathbf{a}_{\setminus i}] - \frac{1}{8} \sum_{j \neq i}^{1,N} a_j H_j[\mathbf{a}_{\setminus j}] + \text{c.c.} \quad (14) \\ &= \mathcal{H}_i[a_i|\mathbf{a}_{\setminus i}] + \mathcal{H}_{\setminus i}[\mathbf{a}_{\setminus i}] \end{aligned}$$

In terms of this decoupling the partition function reads:

$$Z = \sum_{\mathbf{a}_{\setminus i}} \exp \{-\beta\mathcal{H}_{\setminus i}[\mathbf{a}_{\setminus i}]\} Z_i[\mathbf{a}_{\setminus i}] \quad (15)$$

with

$$Z_i[\mathbf{a}_{\setminus i}] \equiv \sum_{a_i} \exp \{a_i H_i[\mathbf{a}_{\setminus i}] + \text{c.c.}\} \quad (16)$$

In order to effectively carry out the sum over a_i values one has to recall that the phasors satisfy a global *spherical* constraint $\sum_j |a_j|^2 = \epsilon N$, with constant ϵ . Once all $\mathbf{a}_{\setminus i}$ are given, then, the value of $|a_i|$ is fixed,

$$|a_i| = \sqrt{\epsilon N - \sum_{j \neq i} |a_j|^2} \quad (17)$$

and \sum_{a_i} simply reduces to an integral on the angular phase variable $\phi_i \in [0 : 2\pi[$. Using Eqs. (14) and (15) the likelihood function of the values of a_i , biased by $\mathbf{a}_{\setminus i}$ values, can be written, eventually, as

$$P_i(a_i|\mathbf{a}_{\setminus i}) = \frac{1}{Z_i[\mathbf{a}_{\setminus i}]} \exp \{a_i H_i[\mathbf{a}_{\setminus i}] + \text{c.c.}\} \quad (18)$$

In order to find the best estimates of the interaction parameters given M mode amplitude configurations we minimize the log-pseudolikelihood functional $-\mathcal{L}_i$:

$$-\mathcal{L}_i = -\sum_{\mu=1}^M \left(a_i^\mu H_i[\mathbf{a}_{\setminus i}^\mu] + \text{c.c.} \right) + \sum_{\mu=1}^M \ln Z_i[\mathbf{a}_{\setminus i}^\mu] \quad (19)$$

with respect to the coupling parameters. In order to perform an optimized procedure we minimize $-\mathcal{L}_i$ functions exploiting the explicit knowledge of the derivatives, i.e.,

$$\frac{\partial(-\mathcal{L}_i)}{\partial J_{ijkl}} = \sum_{\mu=1}^M \mathcal{F}_{jkl}^\mu [\langle a_i \rangle_i^\mu - a_i^\mu] \quad (20)$$

where we denoted

$$\langle (\dots) \rangle_i \equiv \frac{1}{Z_i[\mathbf{a}_{\setminus i}^\mu]} \sum_{a_i} (\dots) \exp \left\{ a_i H_i[\mathbf{a}_{\setminus i}^\mu] + \text{c.c.} \right\} \quad (21)$$

Rewriting the complex amplitude in polar coordinates $a_i = A_i e^{i\phi_i}$ we have the following expression for the marginal

$$\begin{aligned} P_i(A_i, \phi_i | \mathbf{A}_{\setminus i}, \phi_{\setminus i}) &= \frac{\exp \left\{ A_i [H_i^R \cos \phi_i + H_i^I \sin \phi_i] \right\}}{Z_i[\mathbf{A}_{\setminus i}, \phi_{\setminus i}]} \\ &= \frac{\exp \left\{ A_i |H_i| \cos(\phi_i - \gamma_i) \right\}}{2\pi \int dA_i I_0(A_i |H_i|)} \end{aligned} \quad (22)$$

where

$$|H_i| = \sqrt{(H_i^R)^2 + (H_i^I)^2} \quad (23)$$

$$\gamma_i = \arctan \frac{H_i^I}{H_i^R} \quad (24)$$

and $I_0(x)$ is the modified Bessel function of the first kind.

As mentioned in the main text, the polar coordinates are most useful in the cases of intensity equidistribution among the modes, $A_i \simeq 1, \forall i$, and of quenched amplitudes, i.e., when the A_i dynamics is quenched on the time scales of the ϕ 's dynamics. In the latter case all A 's can be taken care of by rescaling the coupling constants as $A_i A_j A_k A_l J_{ijkl} \rightarrow J_{ijkl}$. When the couplings are considered real-valued, the polar expressions of the local effective fields in Eq. (7) can be rewritten by substituting Eq. (8) with

$$\begin{aligned} \mathcal{F}_{jkl}^R &= \cos \phi_j \cos \phi_k \cos \phi_l + \frac{1}{3} (\cos \phi_j \sin \phi_l \sin \phi_k \\ &\quad + \cos \phi_l \sin \phi_j \sin \phi_k + \cos \phi_k \sin \phi_j \sin \phi_l) \end{aligned} \quad (25)$$

$$\begin{aligned} \mathcal{F}_{jkl}^I &= \sin \phi_j \sin \phi_k \sin \phi_l + \frac{1}{3} (\sin \phi_j \cos \phi_l \cos \phi_k \\ &\quad + \sin \phi_l \cos \phi_j \cos \phi_k + \sin \phi_k \cos \phi_j \cos \phi_l) \end{aligned} \quad (26)$$

and the log-pseudolikelihood functional \mathcal{L}_i and its gra-

dient, cf. Eqs. (19,20), simplify to

$$-\mathcal{L}_i = \sum_{\mu=1}^M \left\{ \ln 2\pi I_0 \left(|H_i(\phi_{\setminus i}^\mu)| \right) - \left[H_i^R(\phi_{\setminus i}^\mu) \cos \phi_i^\mu + H_i^I(\phi_{\setminus i}^\mu) \sin \phi_i^\mu \right] \right\} \quad (27)$$

$$\begin{aligned} \frac{\partial(-\mathcal{L}_i)}{\partial J_{ijkl}} &= \sum_{\mu=1}^M \left\{ \mathcal{F}_{jkl}^\mu \right. \\ &\quad \times \left. \left[\frac{I_1(|H_i(\phi_{\setminus i}^\mu)|)}{I_0(|H_i(\phi_{\setminus i}^\mu)|)} \frac{H_i(\phi_{\setminus i}^\mu)}{|H_i(\phi_{\setminus i}^\mu)|} - e^{i\phi_i^\mu} \right] + \text{c.c.} \right\} \end{aligned} \quad (28)$$

To determine the interaction network of non-linear wave systems we compared two techniques: the ℓ_1 -regularization PLM [40, 41] and the decimation PLM [42].

ℓ_1 -regularization In this approach we add a ℓ_1 norm contribution for each coupling to be inferred to the log-likelihood in order to keep the coupling values from diverging during the inference iterative procedure:

$$\mathcal{L}_i \rightarrow \mathcal{L}_i - \lambda_J \sum_{jklm}^{\text{d.i.}} |J_{jklm}| \quad (29)$$

The regularizer λ_J must be small in order to prevent the modification of the landscape of \mathcal{L}_i . We took a pseudolikelihood intensive in M but small enough values of λ_J for all M 's.

Within this method for each mode i all couplings involving i are inferred in one apart iteration. The same quadruplet can, thus, be inferred more times, proceeding by minimizing likelihood functions for different, though interacting, modes and nothing prevents the values of apart reconstructions to be the same. Eventually, thus, all inferred values of the same coupling are averaged in order to enforce the original symmetry.

A further improvement in the reconstruction of the topology can be achieved, as suggested in Ref. [41], by setting to zero all couplings whose estimate is below a threshold value δ . However, the choice of the δ value might be delicate since there are many cases in which there is no clear gap between the zero and the non-zero couplings [42]. If the probability distributions of the estimators are known, we can overcome this problem developing a more accurate hypothesis testing scheme. It can be seen that, as $M \rightarrow \infty$, the probability distribution of the maximum PL estimator converges to a Gaussian distribution centered around the true value of the coupling and with variance estimated by the diagonal elements of the inverse of the Fisher information matrix [51]. The elements, \mathcal{I}_{ab}^i , of the Fisher information matrix are defined

through:

$$\mathcal{I}_{ab}^i = - \left. \frac{\partial^2 \mathcal{L}_i}{\partial J_a \partial J_b} \right|_{\hat{\mathbf{j}}} \quad (30)$$

where with a, b we indicate two possible quadruplets node i might belong to, i.e., $\mathcal{I}_{ab}^i \equiv \mathcal{I}_{jkl, j'k'l'}$. Then, knowing the distribution, we can determine, for every estimated value, if it is compatible with a Gaussian centered in zero, i.e., if the hypothesis for the true coupling to be zero might or not be rejected. The hypothesis testing can then be developed as follows.

- (i) Once the maximum points of the PL are found, we evaluate the inverse of the Fisher information matrix, Eq. (30); from Eq. (27), we have:

$$\begin{aligned} \mathcal{I}_{ab}^i = \sum_{\mu=1}^M \mathcal{F}_a^\mu \mathcal{F}_b^\mu & \left\{ \right. \\ & \times \left(\frac{H_i(\phi_{\setminus i}^\mu)}{|H_i(\phi_{\setminus i}^\mu)|} \right)^2 \mathcal{B} \left(|H_i(\phi_{\setminus i}^\mu)| \right) \\ & \left. + \frac{I_1(|H_i(\phi_{\setminus i}^\mu)|)}{I_0(|H_i(\phi_{\setminus i}^\mu)|)} \left(\frac{|H_i(\phi_{\setminus i}^\mu)|^2 - (H_i(\phi_{\setminus i}^\mu))^2}{|H_i(\phi_{\setminus i}^\mu)|^3} \right) \right\} \end{aligned} \quad (31)$$

where with $\mathcal{B}(x)$ we indicate:

$$\mathcal{B}(x) = \frac{1}{2} \left(\frac{I_2(x)}{I_0(x)} + 1 \right) - \left(\frac{I_1(x)}{I_0(x)} \right)^2$$

the diagonal terms of the inverse matrix are taken as estimates for the variances, $\hat{\sigma}_a$, of the estimator distributions.

- (ii) We assume every couplings to be zero; hence, we expect every estimated value a to be compatible with $N(0, \hat{\sigma}_a)$ distribution. We, then, construct a confidence interval C_n that contains the estimated value \hat{J}_a within a 97.5% probability.
- (iii) If the inferred \hat{J}_a is contained in C_n we cannot reject the zero hypothesis and the coupling is set to zero.

PLM Decimation In the decimation procedure we maximize the total log-likelihood for all modes

$$\mathcal{L} \equiv \frac{1}{N} \sum_i^N \mathcal{L}_i \quad (32)$$

starting from \mathcal{L}_{\max} defined on a full graph and inferring all the values of the $N_q \sim N^4$ couplings on that network. Sorting the couplings by their absolute value and

taking away the N_0 smallest we are left with a network of $N_q - N_0 = xN_q$ non-zero couplings. A new inference iteration, including minimization of $\mathcal{L}(x)$ and sorting, will allow to decimate further another group of the smallest couplings. And so on and so forth, as far as the couplings of the decimated model network are more than the couplings of the true system. Indeed, as far as the number of inferred parameters is larger than the true number of parameters the likelihood is not expected to change and will stick to its maximum value \mathcal{L}_{\max} (overfitting). The indication of the true number of couplings will be given, indeed, right by the x value of the fraction of non-decimated couplings across which \mathcal{L} starts decreasing because the number of inferred parameters is less than the real number of parameters (underfitting). The minimum conceivable $\mathcal{L}(x)$ is for the non-interacting system: $\mathcal{L}_{\min} = \mathcal{L}(0)$. To enhance the determination of the true network connectivity $x_{t.n.}$, below which statistical interpolation becomes less reliable, Decelle and Ricci-Tersenghi [42] introduced the *tilted* pseudolikelihood \mathcal{L}_t

$$\mathcal{L}_t \equiv \mathcal{L}(x) - x\mathcal{L}_{\max} - (1-x)\mathcal{L}_{\min} \quad (33)$$

such that

$$\begin{aligned} \mathcal{L}_t(0) &= \mathcal{L}_t(1) = 0 \\ \mathcal{L}_t(x \leq x_{t.n.}) &\simeq x(\mathcal{L}_{\max} - \mathcal{L}_{\min}). \end{aligned}$$

We stress that using the total likelihood, cf. Eq. (32), the symmetry of coupling constants under indices permutation is automatically enforced.

Erdos-Renyi and Mode-locked graphs We report the distributions of connectivities in the various graphs that we used to test the reconstruction methods exposed in the main manuscript for the models Eq. (1) and Eq. (4) at finite N . In the spherical models (SM) of phasors, cf. Eq. (1), where the total number of couplings scales like N^3 the x axis is the connectivity per variable nodes rescaled by N^2 .

The distributions in the ER-like graphs and in the ML-like graphs in pairwise interacting systems are known to tend to Poissonian distributions in the thermodynamic limit $N \rightarrow \infty$ [55], though the ML-graph convergence is much slower in increasing N . As a comparison, in

N	phasor ER	phasor ML	XY ER	XY ML
16	$N_q = 366$	$N_q = 252$	$N_q = 48$	$N_q = 47$
32	$N_q = 2949$	$N_q = 2360$	$N_q = 96$	$N_q = 72$
128	$N_q = 188742$	$N_q = 168672$	$N_q = 384$	$N_q = 275$

TABLE I. Total number of quadruplets in all simulated networks used to yield data to be tested by our pseudolikelihood inference methods.

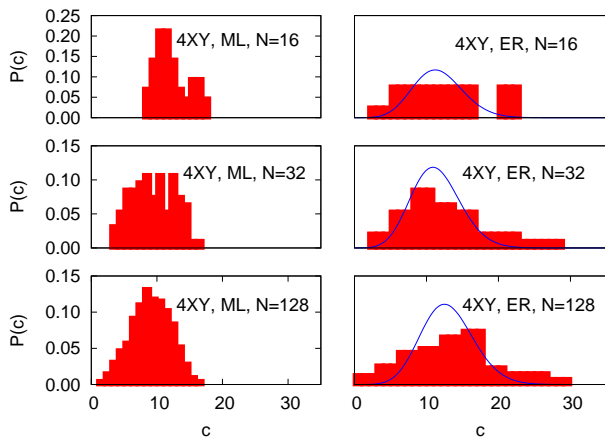


FIG. 7. Distribution of connectivity per variable node of the 4XY models on ER-like (left) and Mode-Locking-like (right) sparse graphs of sizes $N = 16, 32, 128$. The blue curves in the right panels are Poisson distributions with same mean as the empirical distributions.

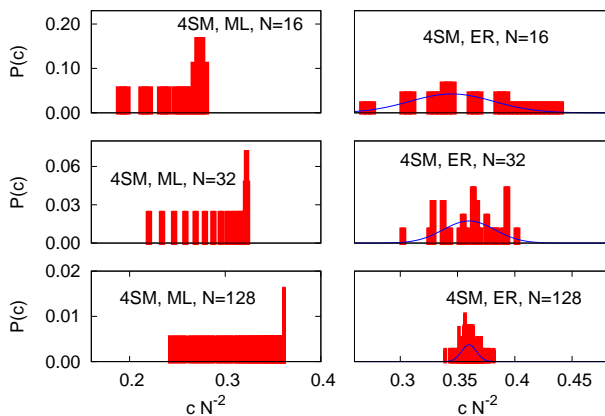


FIG. 8. Distribution of rescaled connectivity c/N^2 in the 4-phasor models - termed "spherical model" (SM) in the plots - on ER-like and ML-like dense ($O(N^3)$) graphs of sizes $N = 16, 32, 128$. The blue curves in the right panels are Poisson distributions with same mean as the data derived distributions.

the right panels of Figs. 7, 8 we plot the relative Poissonian distributions finite sizes. Finite size effects are clearly strong for the simulated sizes, both for the pairwise cases and for the 4-body cases. The actual number of couplings for each simulated instance is reported for all considered models in Tab. I.

Finite size critical temperature. We refer several times to a critical region in T for which inference works better

that at higher, or lower, T . In particular, the reconstruction error is up to one order of magnitude smaller and

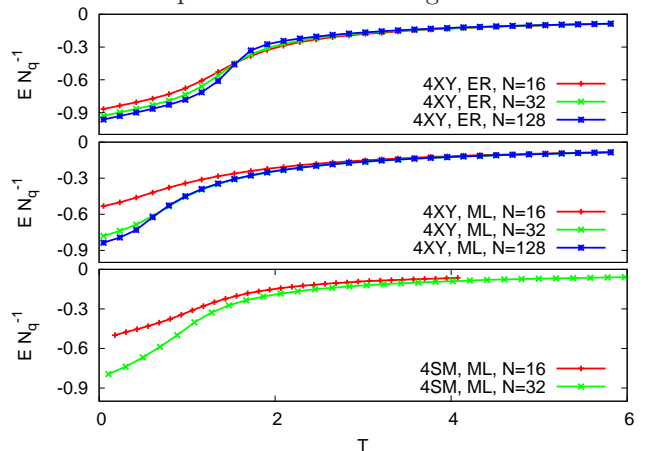


FIG. 9. Internal energy vs. temperature in various simulated instances of the models of Eqs. (1,4)

the network topology is correctly reconstructed with the need of less configurations data. In Fig. 9 we display the energy plots of the models used to produce data with Exchange Monte Carlo simulations. In the thermodynamic limit $N \rightarrow \infty$ they should display a true critical point behavior where a phase transition occurs from a paramagnetic-like phase to a phase-locked or to a spin-glass phase. For the 4XY model on ER-like sparse graphs these temperatures are analytically known, as $T_c = 0$ for $N_q/N = 1$ and $T_c > 0$ for $N_q/N = 2$ [45]. For finite sizes the mathematical discontinuity is approximated by a steep, though smeared, descent lowering T . This step becomes steeper and steeper as N increases eventually reaching the limit of a true singularity representing a true phase transition. Indeed, for finite systems, no actual phase transition occurs. However, one can identify finite size pseudocritical points that, for various systems of increasing size N , form a series converging to the true critical point. Operatively we take as finite size critical points $T_c(N)$ the peak of the specific heat dE/dT from $E_N(T)$ data in Fig. 9. For the simulated systems reported in Fig. 9 they are reported in Tab. II.

N	phasor ML	XY ER	XY ML
16	1.07(1)	1.34(1)	0.50(1)
32	0.91(1)	1.39(1)	0.72(1)
128		1.53(1)	0.63(1)

TABLE II. Finite size proxies for the critical point.